PCCP

ROYAL SOCIETY OF CHEMISTRY

PAPER

View Article Online
View Journal

Cite this: DOI: 10.1039/d5cp01911g

Efficient capture and conversion of H_2S into H_2 and sulfur in guanidinium ionic liquid–NaOH aqueous solution

Qianqian Peng,†[ab] Chengxuan Zhou,†[a] Shucan Qin,[ab] Jinbiao Liang,[b] Shengyun Xu,[ab] Jiaming Mao,[bd] Jianming Shi,[c] Yanrong Liu *[bde] and Yunqian Ma *[abc]

Electrochemistry allows for the simultaneous conversion of hydrogen sulfide (H_2S) to hydrogen (H_2) and sulfur, achieving atomic economy, and is a sustainable and cost-effective method. At the same time, an electrolyte with high conductivity and H_2S absorption that can effectively capture H_2S in an electrochemical process is essential. An ionic liquid electrolyte system for the absorption and electrolysis of H_2S was constructed using the guanidine salt ionic liquid with amine-based functional groups as the carrier electrolyte, water as the solvent, and NaOH as the H_2S absorber. The prepared electrolyte ([TMG][IM]-AE-30) showed a strong absorption of H_2S with an equilibrium solubility of 100.82 g L^{-1}. Under constant potential electrolysis at 1.0 V *vs.* RHE, the maximum hydrogen production rate reaches 2919.97 μmol h^{-1} and the Faraday efficiency reaches 99%, and the anodic product is α-sulfur with a production of 0.881 g after electrolysis for 8 h; the current density and hydrogen production rate are still higher than those of the AE systems after three cycles. Overall, the system has good hydrogen sulfide absorption and electrolysis performances, and [TMG][IM] can effectively improve the H_2S absorption and electrolysis efficiencies.

Received 21st May 2025,
Accepted 1st August 2025

DOI: 10.1039/d5cp01911g

rsc.li/pccp

1. Introduction

Hydrogen sulfide (H_2S), an extremely irritating, foul-smelling and toxic chemical, is present as an impurity in many kinds of important fuel gases, contributing to naturally occurring sulfur emissions in the atmosphere, leading to environmental pollution and life-threatening hazards.[1,2] To treat H_2S, the current industrial technology is mainly based on the Claus process primarily, in which H_2S is catalytically converted to the element sulfur, but the hydrogen element in H_2S is ultimately wasted as water.[3–6] Due to thermodynamic limitations, H_2S cannot be completely converted in the Claus process, therefore, additional purification processes, such as absorption by alkanolamine solutions[7] and selective catalytic oxidation by metal oxides[8] or activated carbons,[9] are required to remove residual H_2S from the Claus tail gas,[10] also without stabilization of hydrogen components. The high calorific value hydrogen resource is a clean fuel and one of the most promising candidates as a sustainable green energy carrier.[11–13] Therefore, cost-effective and sustainable methods for simultaneous conversion of H_2S into H_2 and sulfur with atomic economy are highly desirable.

Extensive research has been conducted over the years to obtain high conversion rates for H_2S decomposition through pyrolysis,[14,15] photolysis,[16,17] electrolysis,[18–22] plasma-assisted conversion,[23–25] microwave-assisted reactions,[26,27] superadiabatic combustion,[28] biolysis,[29,30] *etc.* Compared with the other H_2S decomposition technologies, H_2S electrolysis is more economically viable, which can recover H_2 at the cathode and S at the anode, where the sulfion oxidation reaction (SOR: $S_2^- \rightarrow S + 2e^-$, $E = -0.48$ V *vs.* SHE) is more thermodynamically favorable than the oxygen evolution reaction (OER: $4OH^- \rightarrow O_2 + 2H_2O + 4e^-$, $E = 0.40$ V *vs.* SHE) for water splitting.[31–33] Most researchers pay attention to the SOR using Na_2S and NaOH as anolytes,[34,35] while the pre-H_2S absorption is ignored. Efficient capture of H_2S using electrochemical technology is of great importance, due to the concentration of H_2S and the form

[a] College of Environmental Science and Engineering, Qilu University of Technology (Shandong Academy of Science), Jinan, 250353, PR China. E-mail: mayq@qlu.edu.cn
[b] Longzihu New Energy Laboratory, Zhengzhou Institute of Emerging Industrial Technology, Henan University, Zhengzhou, 450000, PR China
[c] Mingshuo Environment Technology Group Co., Ltd, Weifang, 262605, PR China
[d] CAS Key Laboratory of Green Process and Engineering, State Key Laboratory of Mesoscience and Engineering, Beijing Key Laboratory of Ionic Liquids Clean Process, Institute of Process Engineering, Chinese Academy of Sciences, Beijing, 100190, PR China
[e] School of Chemical Engineering, University of Chinese Academy of Sciences, Beijing, 100049, PR China
† Q. Peng and C. Zhou authors contributed equally to this work.

of the reactant, therefore, a kind of electrolyte with high electrical conductivity and high H_2S absorption capacity that can switch between absorption and electrolysis is essential.

Ionic liquids (ILs), as a new medium, have shown unique advantages in the field of gas absorption and separation as well as electrochemistry.[36–39] The interactions between ILs and H_2S have been confirmed, and the performance of H_2S absorption and separation can be enhanced through functionalized design.[40–49] It has been reported that carboxylate-functionalized ILs,[40] dual Lewis base (DLB)-functionalized ILs,[46] and azole-derived protic ionic liquids (PILs)[42] have high absorption capacities for H_2S. ILs with 1,1,3,3-tetramethylguanidine and its derivatives as cations are called guanidinium ILs, and they all have an amine structure ($-NH_2$), and the nitrogen atoms on the amine group possess a strong electronegativity and strong hydrogen bonding, which allow H_2S to interact with them and enhance the absorption capacities. Currently, SO_2 absorption has been studied by the guanidinium IL, whose amino group in the cation reacts with SO_2 for desulfurization.[50–52] Wu *et al.*[51] have first used 1,1,3,3-tetramethylguanidine lactate ([TMG]L) for SO_2 absorption, and the results showed that 1 mol of [TMG]L could absorb 0.978 mol of SO_2 from a mixture of SO_2 and N_2 at ambient pressure and 40 °C, and the absorbed SO_2 could then be reversibly desorbed in a vacuum or by heating. However, these guanidinium ILs are rarely used for H_2S absorption. Huang *et al.*[52] have prepared a series of phenolic ILs containing different cations and investigated H_2S and CO_2 adsorption performance, which showed that [TMGH][PHO] has high H_2S solubility and high H_2S/CO_2 selectivity due to the strong basicity of its anion and the strong ability of its cation to contribute to hydrogen bonding. With a wide electrochemical window and high ionic conductivity, ILs have been used as electrolytes in many electrochemical processes.[53] For H_2S electrolysis, ILs have been reported as supporting electrolytes to organic electrolytes. These IL based organic electrolytes were composed of TGDE, MEA and $[C_3OHmim]BF_4$, and were proved to be dependent on the sulfur solubility at high temperature with absorption effects of MEA in the system, in favor of solving passivation problems.[54] However, there is no report on the use of ionic liquids in aqueous electrolytes for H_2S electrolysis or the SOR. Since specific functionalized ILs have good absorption capacities for H_2S, they help promote the electrocatalytic H_2S decomposition reaction and improve the yield of products at both the anode and cathode in IL based aqueous electrolytes. Therefore, the absorption and electrolysis can be further intensified by ILs for highly efficient capture and conversion of H_2S, which is superior to the Claus process.

In this study, an ionic liquid–NaOH aqueous solution was used for the first time as both an absorbent and an electrolyte for efficient valorization of H_2S in an electrochemical method. A series of guanidinium ILs (Fig. 1) were selected to design advanced desulfurization solutions. H_2S absorption capacities by the desulfurization solutions were evaluated, and the electrochemical performances for H_2S decomposition on a plain carbon cloth were tested, using the desulfurization solution saturated with H_2S as the anode electrolyte, and the product rate and Faraday efficiency of sulfur and H_2 were calculated.

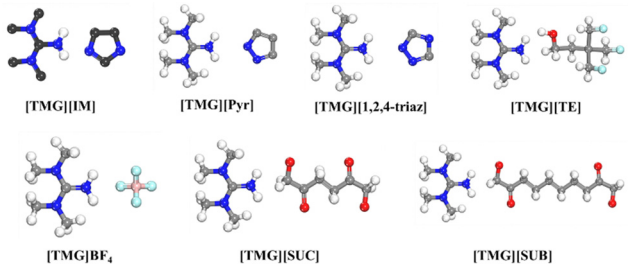

Fig. 1 Chemical structures of a series of guanidinium ionic liquids.

The anion species and the content of guanidinium ILs were optimized to regulate the absorption and electrolysis of H_2S.

2. Materials and methods

2.1. Materials

1,1,3,3-Tetramethylguanidine ($C_5H_{13}N_3$, TMG), imidazole ($C_3H_4N_2$, IM), 2,2,2-Trifluoroethanol ($C_2H_3F_3O$, TE), pyrazole ($C_3H_4N_2$, Pyr), 1,2,4-Triaz ($C_2H_3N_3$), suberic acid ($C_8H_{14}O_4$, SUB) and succinic acid ($C_4H_6O_4$, SUC) were purchased from Adamas, and tetrafluoroboric acid (HBF_4) was obtained from Aladdin. Sodium hydroxide (NaOH), sulfuric acid (H_2SO_4), and ethanol (CH_3CH_2OH) were purchased from Adamas. The H_2S standard gas (1%, N_2 as the carrier gas) was supplied by Henan Yuanzheng Special Gas Co., LTD.

2.2. Preparation of ILs

The ILs [TMG][IM], [TMG][SUC] and $[TMG]BF_4$ were synthesized according to the established method described in the literature. [TMG][IM] was synthesized *via* direct neutralization of TMG and imidazole.[50,55] Briefly, 11.52 g (0.10 mol) of TMG was placed in a 25 mL round bottom flask, and then an equal molar amount of imidazole was added and the mixture was stirred in a magnetic agitator at room temperature for 12 h, and finally [TMG][IM] was obtained. The synthetic method of [TMG][TE], [TMG][1,2,4-triaz] and [TMG][Pyr] is similar to that of [TMG][IM]. In order to synthesize [TMG][SUC],[56] 1,1,3,3-tetramethylguanidine (11.52 g, 0.10 mol) was weighed into a 100 mL round bottom flask and dissolved by adding 40 mL of absolute ethanol. Then, succinic acid (5.90 g, 0.05 mol) was added gradually under magnetic stirring, and the reaction was stopped after stirring for 24 h at room temperature. A white solid was obtained after the solvent was removed by rotary evaporation. Finally, the IL [TMG][SUC] was obtained by drying for 24 h under vacuum. The synthesis method of [TMG][SUB] is similar to that of [TMG][SUC]. To prepare $[TMG]BF_4$,[57] the concentrated 50% HBF_4 (17.60 g, 0.10 mol) was slowly added to the stirred TMG (11.50 g, 0.10 mol) in ethanol solution (100 mL) while cooling in an ice bath. After continuous stirring (298 K, 24 h), the liquid was heated and dried at 343 K under reduced pressure (1 mbar), and finally the colorless and viscous ionic liquid was obtained.

2.3 H_2S absorption experiments

The H_2S absorbent, described as the IL based aqueous electrolyte or ionic liquid–NaOH aqueous solution, consisted of the

synthesized guanidinium IL (from 10 wt% to 50 wt%) and sodium hydroxide aqueous solution (1.0 mol L^{-1}), named as IL-AE-*x* (*x* = 10, 20, 30, 40, and 50). Moreover, the 30 mL of IL-AE was treated under ultrasound for 30 min before bubbling with H_2S gas. After being saturated with H_2S or ventilated with N_2 for 30 min without H_2S, the expended or pristine absorbents were used as the anolyte.

The H_2S absorption capacity was tested by continuously bubbling H_2S standard gas (1%, N_2 as the carrier gas) at room temperature with a flow rate of 100 mL min^{-1} through a gas absorbent bottle containing IL-AE until H_2S appeared in the outlet gas. The concentration of H_2S was detected by a portable hydrogen sulfide gas analyzer (MIC600). The gas flowmeter (D08-1F) from Beijing Seven Star Flow Co., LTD was used to control the quantitative and constant flow rate of the H_2S standard gas. The time that it takes for H_2S to enter and eventually penetrate the electrolyte is called the breakthrough time. The removal efficiency of H_2S is calculated using eqn (1).

$$H_2S\ \text{removal efficiency} = \frac{C_{in} - C_{out}}{C_{in}} \times 100\% \qquad (1)$$

where C_{in} and C_{out} represent the inlet concentration (mg m^{-3}) and the outlet concentration of H_2S, respectively.

2.4. Electrochemical experiment

In the H_2S electrochemical decomposition experiment, a H-type cell and a three-electrode system were used in the electrochemical workstation (CHI660e), and the H-type cell is divided into a cathode chamber and an anode chamber, which were separated by a Nafion 117 proton exchange membrane. In this three-electrode system, a carbon cloth (1 × 1 cm^2), Hg/HgO and a platinum sheet (1 × 1 × 0.02 cm^3) were used as the working electrode, reference electrode and the counter electrode, respectively. 30 mL of IL-AE with saturated H_2S and 30 mL of 0.5 mol L^{-1} H_2SO_4 solution were used as the anolyte and catholyte, respectively.[21]

Firstly, the electrolysis performance of H_2S was evaluated by linear sweep voltammetry (LSV). Slow magnetic agitation was applied during the scanning process to make the anodic solution more uniform and stable. The anodic polarization curves were obtained at a scanning rate of 5 mV s^{-1} and at the scanning potential ranging from 0 V to 1 V (*vs.* RHE). The products were studied by constant potential electrolysis. During the electrochemical reaction, the gas product at the cathode was collected using gas collection bags, and the qualitative and quantitative analysis was carried out by gas chromatography (8860 GC system, Agilent). The solid products at the anode, obtained through acidification and filtration of the anode electrolyte IL-AE, were analyzed quantitatively and qualitatively.

The hydrogen production rate was calculated using eqn (2).

$$\text{Rate}_{H_2} = \varphi_{H_{2n}} \times \text{flow rate} \times \frac{P_0}{RT} \qquad (2)$$

where $\varphi_{H_{2n}}$ represents the volume fraction of H_2 in the tail gas at the *n*th hour in the process of electrolysis, which can be calculated using the calibration curves of the GC; R = 8.314 J (mol K)$^{-1}$; P_0 = 1.013 bar and T = 298.15 K; and the flow rate is the rate at which gas enters the system.

The Faraday Efficiency of the gas product H_2 per hour (FE_{H_2}) was calculated using eqn (3).

$$FE_{H_2} = \frac{\varphi_{H_{2n}} \times \text{flow rate} \times t_n \times \frac{zFP_0}{RT}}{Q_n} \times 100\% \qquad (3)$$

where *n* is the *n*th hour of electrolysis, here *n* = 8; $\varphi_{H_{2n}}$ is the volume fraction of H_2 in the tail gas at the *n*th hour of electrolysis; t_n is the time at the *n*th hour of electrolysis, here *t* = 1 h; *z* is the number of electrons required to form one molecule of H_2 (here, *Z* = 2); *F* is Faraday's constant, *F* = 96 485 C mol^{-1}; and Q_n is the value of the Coulomb charge transferred at the *n*th hour of electrolysis.

3. Results and discussion

3.1. Screening of guanidinium ionic liquids in IL-AEs

3.1.1. H_2S absorption capacities of IL-AEs. In order to compare the H_2S absorption capacities of different ILs ([TMG][IM], [TMG][TE], [TMG][1,2,4-triaz], [TMG][Pyr], [TMG][SUC], [TMG][SUB] and [TMG]BF_4), the H_2S removal efficiency and equilibrium solubilities of IL-AEs were measured. Fig. 2(a) shows that the H_2S removal efficiencies of [TMG][IM]-AE, [TMG][TE]-AE and [TMG][Pyr]-AE were significantly higher than those of the other four IL-AEs, and [TMG][Pyr]-AE had the highest H_2S absorption capacity with a breakthrough time of more than 960 min. In Fig. 2(b), it is further shown that at normal temperature and pressure, the H_2S equilibrium solubility of [TMG][Pyr]-AE reached the maximum (50 g L^{-1}), and the H_2S equilibrium solubility of [TMG][IM]-AE and [TMG][TE]-AE reached 45 g L^{-1} approximately. The equilibrium solubilities of the four alkaline IL-AEs were higher than that of the conventional electrolyte AE.

3.1.2. Electrochemical performance of IL-AEs. Fig. 3(a) shows the linear LSV curves in different H_2S-saturated electrolytes based on guanidinium ILs. It can be observed that the current density of the electrolytic H_2S system regulated by guanidinium IL is significantly higher than that of the single sodium hydroxide electrolytic system, so the high conductivity of these ionic liquids can promote the H_2S electrolytic reaction, and the current density of the electrolytic H_2S system with [TMG][IM]-AE is the highest. The Tafel slopes are plotted and

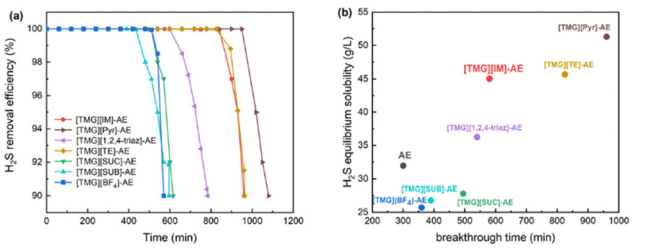

Fig. 2 (a) H_2S removal efficiency of IL-AE, and (b) H_2S breakthrough time and equilibrium solubility of IL-AE.

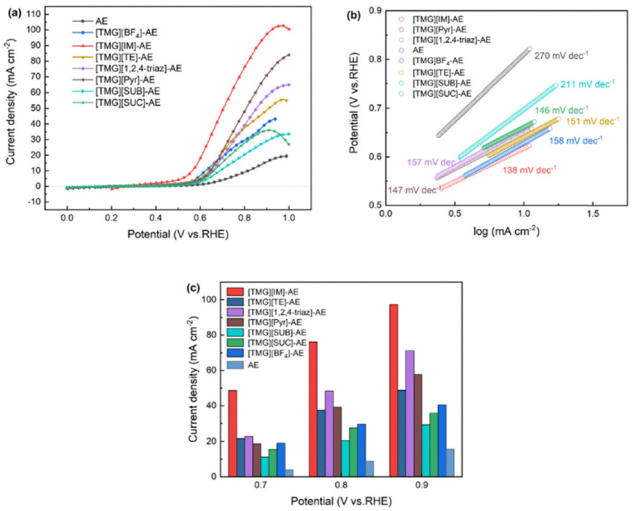

Fig. 3 (a) LSV curves of IL-AE, (b) Tafel slope for SOR of IL-AE, and (c) current densities of IL-AE and AE at 0.7 V, 0.8 V and 0.9 V for the SOR.

analyzed, as shown in Fig. 3(b). Among the IL regulated aqueous electrolytes, the Tafel slope of the anode in [TMG][IM]-AE, 138 mV dec^{-1}, is the smallest one, indicating that [TMG][IM]-AE has favorable catalytic kinetics for the SOR. Fig. 3(c) summarizes the current densities at 0.7, 0.8, and 0.9 V for different ILs-AE. At 0.9 V, the current density of [TMG][IM]-AE can reach up to 97.31 mA cm^{-2} with the carbon cloth as the anode. Although the [TMG][Pyr]-AE system exhibits a strong alkaline advantage in the absorption stage, the unique conjugated planar structure of the imidazole anion endows the IL with high electrical conductivity and excellent charge transport capacity, promoting the improvement of ion migration and electron transfer efficiency during electrolysis. Consequently, [TMG][IM] was selected as the key ionic liquid to regulate the aqueous electrolyte.

3.2. Screening of electrolytes with the [TMG][IM] content

3.2.1. H_2S absorption capacities of [TMG][IM]-AE-*x*. It is found that the aqueous electrolyte with the [TMG][IM] ionic liquid has the best effect on the H_2S absorption capacities and electrochemical performances. Therefore, the effect of different [TMG][IM] contents (10 wt%, 20 wt%, 30 wt%, 40 wt% and 50 wt%) on the SOR was further investigated. In Fig. 4, it is shown that the breakthrough time became longer as the [TMG][IM] contents increase, and the H_2S equilibrium solubility became larger as the [TMG][IM] contents increase. Therefore, 50 wt% is the best [TMG][IM] content, and its breakthrough time and H_2S equilibrium solubility reached 1560 min and 100.82 g L^{-1}, respectively (Fig. 4(b)).

3.2.2. Electrochemical performance evaluation of [TMG][IM]-AE-*x*. Fig. 5(a) shows the LSV curves of [TMG][IM] aqueous electrolytes with different IL contents. The current density reaches the maximum (181.6 mA cm^{-2} at 1.2 V) when the addition amount of the IL is 30 wt%. As shown in Fig. 5(b), the aqueous electrolyte with 30 wt% of the ionic liquid has the lowest Tafel slope, which is only 149 mV dec^{-1}. It was suggested that [TMG][IM]-AE-30 has the fastest electron transfer rate at the

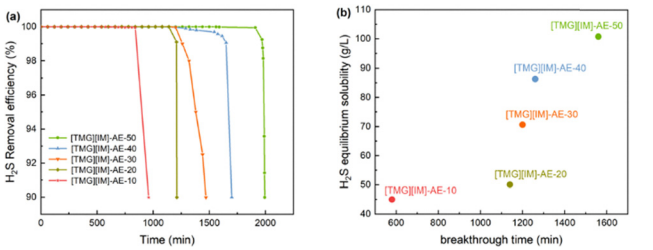

Fig. 4 (a) H_2S absorption capacities of [TMG][IM]-AE-*x*, and (b) H_2S breakthrough times and equilibrium solubilities of [TMG][IM]-AE-*x* (*x* = 10–50).

electrode interface and the best kinetic advantage during the reaction. The increase of the [TMG][IM] content increases the density of imidazole anions in the electrolyte and significantly optimizes the charge transport capacity. Fig. 5(c) summarizes the current densities at 0.7, 0.8, and 0.9 V for [TMG][IM]-AE-*x*. At 0.9 V, the current density of [TMG][IM]-AE-30 can reach as high as 96.34 mA cm^{-2}. The increase in the IL content and the decrease in current density is due to the fact that more anion pairs form a large number of ion clusters, which do not contribute to the conductivity of the solution.

3.3. Product analysis

3.3.1. Anode product. Based on the above analysis of the electrochemical performance in guanidinium IL aqueous electrolytes saturated with H_2S, [TMG][IM]-AE, which has the largest activity, is applied to the H_2S electrolytic process and the product was studied by potentiostatic electrolysis. In order to analyze the speciation of polysulfides, the anolyte was tested by UV-vis spectroscopy, and it was found to show obvious absorption peaks at 300 nm and 370 nm, attributed to the existence of short-chain polysulfide ions (S_2^{2-}–S_4^{2-}) in the electrolyte (Fig. 6(a)).[58,59] Polysulfides were formed as the

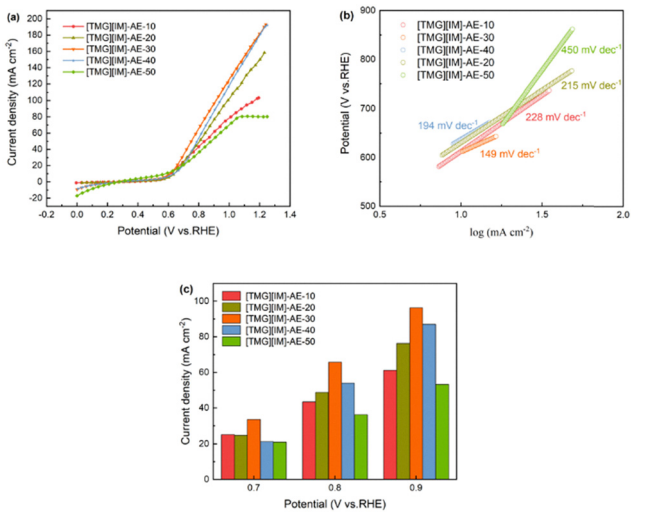

Fig. 5 (a) LSV curves of [TMG][IM]-AE-*x* (*x* = 10–50), (b) Tafel slope for the SOR of [TMG][IM]-AE-*x*, and (c) current densities of [TMG][IM]-AE-*x* at 0.7 V, 0.8 V, and 0.9 V.

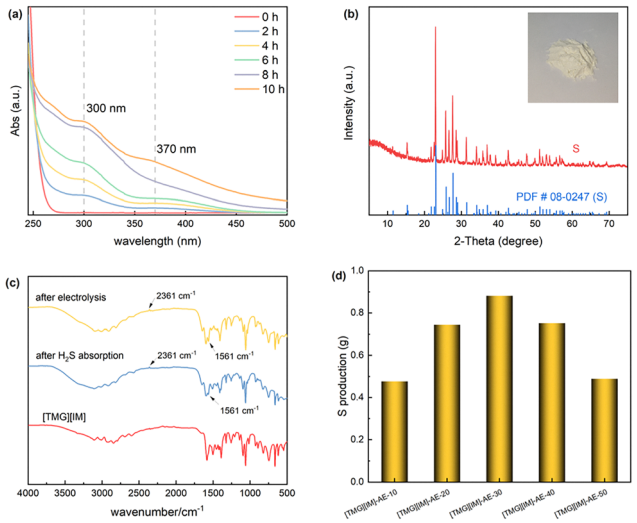

Fig. 6 (a) UV-vis spectrum of [TMG][IM]-AE-30 at different electrolytic times, (b) XRD pattern of the anodic liquid solid product, (c) FI-IR spectrum of [TMG][IM]-AE-30 before and after electrolysis, and (d) sulphur production in [TMG][IM]-AE.

anodic product of sulfur further combining with the sulfide in the electrolyte.[60] Through the acid treatment of the spent anolyte, the yellow precipitate could be efficiently obtained,[61] and then analyzed by XRD (Fig. 6(b)). It was confirmed to be elemental sulfur (α-sulfur), which is the most stable among the three species (α-sulfur, β-sulfur and γ-sulfur), indicating the successful cycling of sulfur in H_2S electrolysis regulated by guanidinium ionic liquids in the anode. As shown in Fig. 6(c), by comparing the FT-IR spectra of [TMG][IM] at different stages, it is found that the electrolyte after absorption and electrolysis of H_2S shows a weak peak at 2361 cm^{-1}, belonging to the S–H stretching vibration, and a peak appeared at 1561 cm^{-1}, which is attributed to the N–H deformation vibration, and a chemical complexation between [TMG][IM] and H_2S is proved. Fig. 6(d) demonstrates the sulfur production of the [TMG][IM]-AE-*x* system, and it can be seen that [TMG][IM]-AE-30 produced the most sulfur at 0.881g, the Sulfur Faraday Efficiency is 72%.

In order to further elaborate the excellent absorption of H_2S by the [TMG][IM]-AE system, DFT calculations were performed. First, a [TMG][IM] structural model was constructed and optimized based on the structures found in the literature (Fig. 7(a)–(c)). Fig. 7(d) shows the adsorption free energies for the three sites on [TMG][IM]. As shown in the figure, [TMG][IM] has excellent adsorption performance for H_2S in the adsorption stage, where the adsorption energies are −1.40 eV for site a, −1.28 eV for site b and −1.57 eV for site c, and it can spontaneously bind to H_2S at ambient temperature and pressure without the need to provide additional energy.

3.3.2. Cathode product. The potential and electrolysis time were set to 1.0 V (*vs.* RHE) and 8 h, respectively, and slow magnetic stirring was applied to the process. From Fig. 8(a), it can be observed that bubbles are generated on the platinum electrode in the cathode chamber. The cathodic product was qualitatively confirmed to be H_2 using a gas chromatograph

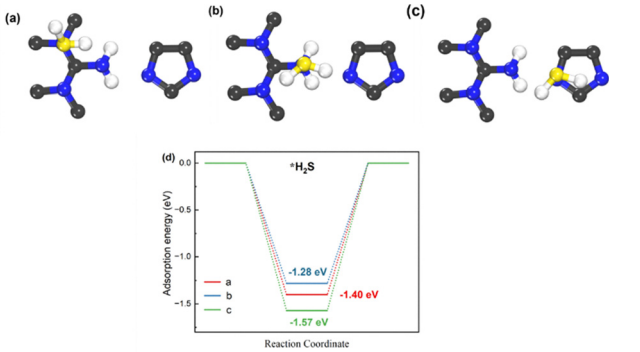

Fig. 7 DFT optimized structures of ionic liquids with (a) adsorption site a, (b) adsorption site b, (c) adsorption site c, and (d) adsorption free energies of H_2S with the three adsorption sites of [TMG][IM].

instrument. As shown in Fig. 8(b) and (c), the H_2S electrolysis system regulated by 30 wt% [TMG][IM] had the highest hydrogen production rate, up to 2919.97 μmol h^{-1}, and the H_2 Faraday efficiency is 99%, which is consistent with that obtained in the electrochemical test discussed in section 3.2.2, and the current density of the [TMG][IM]-AE-30 system is the maximum. As the H_2S electrolysis progressed, the hydrogen production rate of the [TMG][IM]-AE-30 system gradually decreased, which can be attributed to the continuous reduction of the substrate concentration, and this material is not suitable for the reaction at this potential of only 1.0 V (*vs.* RHE).

3.4. Circulation

From the comparison of the performance considering various aspects, [TMG][IM]-AE-30 is found to be the best electrolyte in this study. Therefore, [TMG][IM]-AE-30 was used as the research object to study the circulation performance for H_2S electrolysis. The constant potential electrolysis was carried out at 1.0 V in [TMG][IM]-AE-30 saturated with H_2S. In the process of

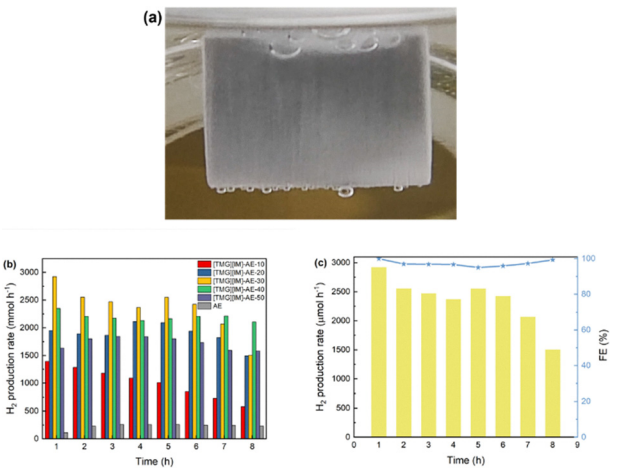

Fig. 8 (a) Bubbles on the platinum electrode of the cathode chamber, (b) hydrogen production rate (per hour) of [TMG][IM]-AE-*x* (*x* = 10–50) in potentiostatic electrolysis at 1.0 V (*vs.* RHE) for 8 h, and (c) hydrogen production rate and Faraday efficiency (per hour) of [TMG][IM]-AE-30 in potentiostatic electrolysis at 1.0 V (*vs.* RHE) for 8 h.

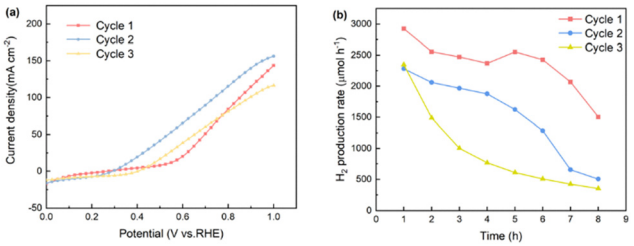

Fig. 9 (a) LSV curves for three cycles, and (b) H_2 production rate for three cycles.

electrolysis, the pH value of the electrolyte changed from 11.03 to 8.74, and the electrolyte volume dropped by around 30%. After 12 h of electrolysis, the pH value was adjusted to 13.96 consistent with that before absorption, and the volume of the electrolyte was also adjusted to 30 mL. Then the next absorption–electrolysis cycle was repeated. The current densities at different potentials and H_2 production rates in each circulation are shown in Fig. 9. At 1.0 V (*vs.* RHE), the current density in the three cycles reached 143.9 mA cm^{-2}, 156.4 mA cm^{-2} and 116.4 mA cm^{-2}, respectively. With an electrolysis duration of 8 h per cycle, the maximum hydrogen production rate decreased from 2925 μmol h^{-1} to 1504 μmol h^{-1} for the first cycle; the maximum hydrogen production rate reduced from 2282 μmol h^{-1} to 506 μmol h^{-1} for the second cycle; the maximum hydrogen production rate for the third cycle decreased from 2347 μmol h^{-1} to 353 μmol h^{-1}. From the FT-IR spectrum (Fig. 6(c)), it can be seen that the IL has changed irreversibly after electrolysis, therefore, the stability of the system is poor, and the electrochemical performance and the production rate of the system decreased, but the measured current densities and hydrogen production rates are still higher than those of conventional AE systems without ILs after three cycles, indicating that the changed IL derivatives still have a promoting effect on the reaction.

3.5. Prospective analysis of industrialization

This technology can be used in the desulphurisation process of natural gas, coal gasification products and petroleum refinery gas, and is expected to replace the traditional Claus process to achieve high-precision removal of high, medium and low concentrations of hydrogen sulfide, and to obtain high-value products: hydrogen and sulfur chemical products. Compared with the traditional Claus process, according to the H_2S treatment capacity of 3000 t per a,[62] the amount of hydrogen produced is 56 t, and the amount of sulfur produced is 1296 t. According to the price of H_2 of 35 CNY per kg and the price of sulfur of 1600 CNY per t, an additional 0.20 million CNY can be added to the income through the production of green hydrogen, and an additional 2.07 million CNY can be generated by high-value sulfur products (no upfront investment cost).

4. Conclusions

In this study, seven guanidine salt-functionalized ILs were prepared and mixed with NaOH aqueous solution in different ratios, which were applied as absorbents and anode electrolytes in the H_2S absorption electrolysis reaction system. Through the screening of different guanidinium salt ILs and the addition amount, [TMG][IM]-AE-30 was found to be the optimal electrolyte system in this study, which was applied as a desulfurizing agent and an anode-loaded electrolyte in the H_2S absorption electrolysis reaction system; the electrochemical performances of the system were evaluated, and the electrolyte had a certain degree of stability. In the electrolysis system, a carbon cloth and a platinum sheet were used as the working and counter electrodes, respectively, without any additional designed catalysts at the anode. The current density of the [TMG][IM]-AE-30 system was maximized to 181.6 mA cm^{-1} and the Tafel slope was minimized to 149 mA dec^{-1}, indicating that it had the fastest reaction rate, which was conducive to electron transfer at the electrode interface. The hydrogen production rate of the [TMG][IM]-AE-30 system reached 2919.97 μmol h^{-1} after electrolysis at a constant potential of 1.0 V for 8 h. High-purity sulfur was extracted from the anode electrolyte by acidification and characterized as α-sulfur by XRD. The S yield after 8 hours of electrolysis was 0.881 g. After three cycles, the electrochemical performance and hydrogen production rate of the system decreased. Through FT-IR characterization, the reason for the decrease is found to be the changes in the guanidine salt ionic liquid after electrolysis. However, the derivatives of the changed guanidine salt ionic liquid still have a promoting effect on the reaction. Therefore, the current density and hydrogen production rate after three cycles are still higher than those of the AE systems.

Author contributions

Qianqian Peng: methodology, investigation, and writing – original draft. Weizhen Kong: methodology and investigation. Shucan Qin: writing – review and editing. Anshuang Wu: methodology. Longmei Shi: investigation. Shengyun Xu: investigation. Jianming Shi: visualization and funding acquisition. Chongqing Xu: formal analysis and funding acquisition. Yanrong Liu: conceptualization, supervision, and writing – review and editing. Yunqian Ma: conceptualization, data curation, supervision, writing – review and editing, and funding acquisition.

Conflicts of interest

There are no conflicts to declare.

Data availability

Data will be available upon reasonable request.

Acknowledgements

This work is supported by the Longzihu New Energy Laboratory, the major innovation projects of science, education, industry

integration of Qilu University of Technology (Shandong Academy of Science) (2022JBZ02-05), the Key R&D Program of Henan Province (No. 231111241800), the National Natural Science Foundation of China (No. 22278402), the Frontier Basic Research Projects of Institute of Process Engineering, CAS (No. QYJC-2023-03), and research fund of State Key Laboratory of Mesoscience and Engineering (No. MESO-23-A08).

References

1 A. Pudi, M. Rezaei, V. Signorini, M. P. Andersson, M. G. Baschetti and S. S. Mansouri, *Sep. Purif. Technol.*, 2022, **298**, 121448.
2 A. G. De Crisci, A. Moniri and Y. Xu, *Int. J. Hydrogen Energy*, 2019, **44**, 1299–1327.
3 M. Zhang, J. Guan, Y. Tu, S. Chen, Y. Wang, S. Wang, L. Yu, C. Ma, D. Deng and X. Bao, *Energy Environ. Sci.*, 2020, **13**, 119–126.
4 M. S. Shah, M. Tsapatsis and J. I. Siepmann, *Chem. Rev.*, 2017, **117**, 9755–9803.
5 E. L. Reddy, V. M. Biju and C. Subrahmanyam, *Int. J. Hydrogen Energy*, 2012, **37**, 2204–2209.
6 M. Lou, R. Wang and H. Song, *Renewable Sustainable Energy Rev.*, 2024, **199**, 114529.
7 R. K. Abdulrahman and I. M. Sebastine, *J. Nat. Gas Sci. Eng.*, 2013, **14**, 116–120.
8 F. Dashtestani, M. Nusheh, V. Siriwongrungson, J. Hongrapipat, V. Materic and S. Pang, *Fuel*, 2021, **295**, 120586.
9 T. J. Bandosz, *J. Colloid Interface Sci.*, 2002, **246**, 1–20.
10 K. Huang, F. Xi, X.-M. Zhang, Y.-T. Wu and X.-B. Hu, *Green Chem.*, 2016, **18**, 1859–1863.
11 S. E. Hosseini and M. A. Wahid, *Renewable Sustainable Energy Rev.*, 2016, **57**, 850–866.
12 S. Wang, Z. Geng, S. Bi, Y. Wang, Z. Gao, L. Jin and C. Zhang, *Green Energy Environ.*, 2024, **9**, 659–683.
13 D. Li, J. Tu, Y. Lu and B. Zhang, *Green Chem. Eng.*, 2023, **4**, 17–29.
14 J. Xu, S. Tang, S. Zhong, L. Song, P. Wu, W. Jiang, K. Wu, Q. Hu, C. Liu, H. Yue, B. Liang and Y. Yang, *Int. J. Hydrogen Energy*, 2023, **48**, 8807–8818.
15 K. M. Kwok, S. W. D. Ong, L. Chen and H. C. Zeng, *ACS Catal.*, 2017, **8**, 714–724.
16 A. Jiang, H. Guo, S. Yu, F. Zhang, T. Shuai, Y. Ke, P. Yang and Y. Zhou, *Appl. Catal., B*, 2023, **332**, 122747.
17 M. Dan, A. Prakash, Q. Cai, J. Xiang, Y. Ye, Y. Li, S. Yu, Y. Lin and Y. Zhou, *Sol. RRL*, 2018, **3**, 1800237.
18 M. Kumar and T. C. Nagaiah, *J. Mater. Chem. A*, 2022, **10**, 13031–13041.
19 Y. Pei, J. Cheng, H. Zhong, Z. Pi, Y. Zhao and F. Jin, *Green Chem.*, 2021, **23**, 6975–6983.
20 S. Zhang, Q. Zhou, Z. Shen, X. Jin, Y. Zhang, M. Shi, J. Zhou, J. Liu, Z. Lu, Y. N. Zhou and H. Zhang, *Adv. Funct. Mater.*, 2021, **31**, 2101922.
21 L. Yi, Y. Ji, P. Shao, J. Chen, J. Li, H. Li, K. Chen, X. Peng and Z. Wen, *Angew. Chem., Int. Ed.*, 2021, **60**, 21550–21557.
22 Y. Li, Y. Duan, K. Zhang and W. Yu, *Chem. Eng. J.*, 2022, **433**, 134472.
23 L. Zhao, Y. Wang, A. Wang, X. Li, C. Song and Y. Hu, *Catal. Today*, 2019, **337**, 83–89.
24 A. Karapekmez and I. Dincer, *Int. J. Hydrogen Energy*, 2018, **43**, 10569–10579.
25 K. Gutsol, R. Robinson, A. Rabinovich, A. Gutsol and A. Fridman, *Int. J. Hydrogen Energy*, 2017, **42**, 68–75.
26 J. Zhu, W. Xu, J. Chen, Z. Gan, X. Wang and J. Zhou, *Catal. Sci. Technol.*, 2020, **10**, 6769–6779.
27 M. Luo, J. Zhou, W. Xu, J. Chen, M. Xiang and K. Peng, *Fuel*, 2020, **281**, 118729.
28 M. Abdul Mujeebu, *Appl. Energy*, 2016, **173**, 210–224.
29 G. Tóth, N. Nemestóthy, K. Bélafi-Bakó, D. Vozik and P. Bakonyi, *Int. Biodeterior. Biodegrad.*, 2015, **105**, 185–191.
30 K. Rana, N. Rana and B. Singh, *Physiological and Biotechnological Aspects of Extremophiles*, 2020, pp. 131–136.
31 W. Wang, Q. Mao, K. Deng, H. Yu, Z. Wang, Y. Xu, X. Li, L. Wang and H. Wang, *Small*, 2023, **19**, 2207852.
32 J. Li, S. Wang, J. Chang and L. Feng, *Adv Powder Mater*, 2022, **1**, 100030.
33 Y. He, Z. Kang, J. Li, Y. Li and X. Tian, *Ind. Chem. Mater.*, 2023, **1**, 312–331.
34 Z. Mao, A. Anani, R. E. White, S. Srinivasan and A. J. Appleby, *J. Electrochem. Soc.*, 1991, **138**, 1299–1303.
35 A. A. Anani, Z. Mao, R. E. White, S. Srinivasan and A. J. Appleby, *J. Electrochem. Soc.*, 1990, **137**, 2703–2709.
36 J. Feng, H. Gao, L. Zheng, Z. Chen, S. Zeng, C. Jiang, H. Dong, L. Liu, S. Zhang and X. Zhang, *Nat. Commun.*, 2020, **11**, 1–8.
37 D. Yang, Q. Zhu and B. Han, *Innovation*, 2020, **1**, 1–25.
38 G. Tian, *Green Sustainable Process for Chemical and Environmental Engineering and Science*, 2021, pp. 149–201.
39 W. Bai, J. Chen, F. Liu, J. Zhang, X. Zhang, Z. Gu and J. Yu, *Phys. Chem. Chem. Phys.*, 2023, **25**, 6295–6305.
40 T. Zhao, P. Li, X. Feng, X. Hu and Y. Wu, *J. Mol. Liq.*, 2018, **266**, 806–813.
41 X. Zhang, W. Xiong, M. Shi, Y. Wu and X. Hu, *Chem. Eng. J.*, 2021, **408**, 127866.
42 W. Zheng, D. Wu, X. Feng, J. Hu, F. Zhang, Y.-T. Wu and X.-B. Hu, *J. Mol. Liq.*, 2018, **263**, 209–217.
43 X. Zhang, W. Xiong, L. Peng, Y. Wu and X. Hu, *AlChE J.*, 2020, **66**, 16936.
44 K. Huang, Y. T. Wu and X. B. Hu, *Chem. Eng. J.*, 2016, **297**, 265–276.
45 K. Huang, J. Y. Zhang, X. B. Hu and Y. T. Wu, *Energy Fuels*, 2017, **31**, 14060–14069.
46 K. Huang, D. N. Cai, Y. L. Chen, Y. T. Wu, X. B. Hu and Z. B. Zhang, *ChemPlusChem*, 2013, **79**, 241–249.
47 W. Xiong, M. Shi, L. Peng, X. Zhang, X. Hu and Y. Wu, *Sep. Purif. Technol.*, 2021, **263**, 118417.
48 K. Huang, X. M. Zhang, X. B. Hu and Y. T. Wu, *AlChE J.*, 2016, **62**, 4480–4490.
49 K. Huang, X. M. Zhang, Y. Xu, Y. T. Wu, X. B. Hu and Y. Xu, *AlChE J.*, 2014, **60**, 4232–4240.
50 Y. Shang, H. Li, S. Zhang, H. Xu, Z. Wang, L. Zhang and J. Zhang, *Chem. Eng. J.*, 2011, **175**, 324–329.

51 W. Wu, B. Han, H. Gao, Z. Liu, T. Jiang and J. Huang, *Angew.Chem.*, 2004, **116**, 2469–2471.
52 K. Huang, X.-M. Zhang, L.-S. Zhou, D.-J. Tao and J.-P. Fan, *Chem. Eng. Sci.*, 2017, **173**, 253–263.
53 Y. Liu, J. Cui, H. Wang, K. Wang, Y. Tian, X. Xue, Y. Qiao, X. Ji and S. Zhang, *Green Chem.*, 2023, **25**, 4981–4994.
54 Y. Ma, X. Jin, Y. Hu, Q. Huang and Z. Wang, *Energy Fuels*, 2020, **34**, 7756–7762.
55 X. Lei, Y. Xu, L. Zhu and X. Wang, *RSC Adv.*, 2014, **4**, 7052–7057.
56 X. Meng, J. Wang, H. Jiang, X. Zhang, S. Liu and Y. Hu, *J. Chem. Technol. Biotechnol.*, 2016, **92**, 767–774.
57 J. Huang, A. Riisager, R. W. Berg and R. Fehrmann, *J. Mol. Catal. A: Chem.*, 2008, **279**, 170–176.
58 C. Barchasz, F. Molton, C. Duboc, J.-C. Leprêtre, S. Patoux and F. Alloin, *Anal. Chem.*, 2012, **84**, 3973–3980.
59 L. Zhang, Z. Wang and J. Qiu, *Adv. Mater.*, 2022, **34**, 2109321.
60 Y. Wu and N. Liu, *Chemistry*, 2018, **4**, 438–465.
61 J. P. Fornés and J. M. Bisang, *Electrochim. Acta*, 2017, **243**, 90–97.
62 C. Duan, C. Tang, M.-N. Wu, S. Yu, T.-J. Yu, H. Guo, J.-J. Li and Y. Zhou, *Natural Gas Chemical Industry*, 2021, **46**, 24–30.

